J Mater Sci (2008) 43:2818–2824
DOI 10.1007/s10853-008-2511-7

Electrical and optical properties of an alcohol soluble aminoalkyl-substituted cationic conjugated polymer

Lin Ke · Vijila Chellappan · Bin Liu · Zhen Xian Soh · Rina Hui Ting Soh · Soo Jin Chua

Received: 30 October 2007 / Accepted: 29 January 2008 / Published online: 28 February 2008

Abstract The optical and electrical properties of a novel alcohol soluble aminoalkyl-substituted cationic conjugated polymer, poly[9,9′-bis(6″-(*N*,*N*,*N*-trimethylammonium)-hexyl) fluorene-*co*-*alt*-2,5-dimethoxy-1,4-phenylene dibromide] (PFPB), has been studied using absorption, photoluminescence, current–voltage–luminescence (*J*–*V*–*L*), and noise characterization techniques. The absorption and photoluminescence studies show that PFPB is blue-emitting, and its long alkyl side chains and two methoxy side chains introduce steric hindrance in the structure, which can minimize interchain interactions. The photoluminescence quantum efficiency of PFPB in methanol was found to be 69.6%. Polymer light emitting diodes (PLEDs) were fabricated using PFPB as an electron injection layer and device physics has been studied. The obtained device results indicate that PFPB can be used as an electron transport layer (ETL) to improve the PLED performance. The noise characteristics on the PLED devices show that the interface between the cathode and the emissive layer is improved through the introduction of a PFPB layer. Results in this report indicate that the poly(fluorene-*co*-phenylene)-based water/alcohol soluble cationic conjugated polymer avoids the intermixing between the electroluminance layer and adjacent ETL layer which is a common and serious problem in multilayer PLED fabrication by solution casting methods. This makes water solubility materials attractive for applications in PLEDs and other organic devices.

L. Ke (✉) · V. Chellappan
Institute of Materials Research and Engineering, 3 Research Link, Singapore 117602, Singapore
e-mail: karen-kl@imre.a-star.edu.sg

B. Liu (✉) · Z. X. Soh · R. H. T. Soh
Department of Chemical and Biomolecular Engineering, National University of Singapore, 10 Kent Ridge Crescent, Singapore 119260, Singapore
e-mail: cheliub@nus.edu.sg

S. J. Chua
Center of Optoelectronics, National University of Singapore, 10 Kent Ridge Crescent, Singapore 119260, Singapore

Introduction

Solid-state light emitting devices have generated wide research interest over the years, and several materials have been tested for application in such devices. With the exception of polyaniline which is soluble in concentrated strong acids [1], the early conjugated polymers are generally insoluble and are obtained as "poorly ordered and noncompact films, whose morphology is determined by the chemical or electrochemical growth conditions and cannot be modified after growth" [2]. Several methods are subsequently developed to counter this problem. The first is to use a soluble precursor polymer as the starting material, and then remove part of the repeat units by thermal processing, thereby retaining the shape and morphology of the precursor polymer while generating a soluble conjugated polymer [3]. However, this is a specific method that depends on the chemical nature of each polymer. A second and more general method is to incorporate bulky substituents such as alkyl chains in each repeat unit. This method was successfully applied to the synthesis of polythiophene in 1986 [4]. An appropriate choice of substituents allows band gap tuning, introduction of "desirable quantities such as chirality, liquid crystalline, or catalytic properties" and even "self-doping" [5]. A third method is to use surfactants or polymer counterions [6]. A fourth and final method is to use a conjugated polymer in conjunction with a

nonconjugated processible polymer either by blending or as a (graft or block) copolymer.

Ionic conjugated polymers have received considerable interest in recent years due to their good solubility in polar solvents. They function as conjugated polyelectrolytes, possessing the ability to combine the optoelectronic and redox properties of traditional conjugated polymers with the aqueous solubility and ionic nature of polyelectrolytes [7]. Other advantages include the use of environmental friendly solvents such as water or alcohols [7] when ionic conjugated polymers are used in device fabrication. Alcohol-soluble conjugated polymers could also be used to construct active layers in polymer light emitting diodes (PLEDs) through a layer-by-layer (LBL) self-assembly approach [7], as buffer layer and emissive layer materials in inkjet printing fabricated PLEDs, and in chemosensor and biosensor applications where an aqueous media and high photoluminescence quantum yield are typically required.

This article reported an undoped alcohol/water-soluble aminoalkyl-substituted cationic conjugated polymer, poly[9,9′-bis(6″-(*N*,*N*,*N*-trimethylammonium)-hexyl)fluorene-*co*-*alt*-2,5-dimethoxy-1,4-phenylene dibromide] [8] (PFPB) and its application as an electron injection layer in organic light emitting devices.

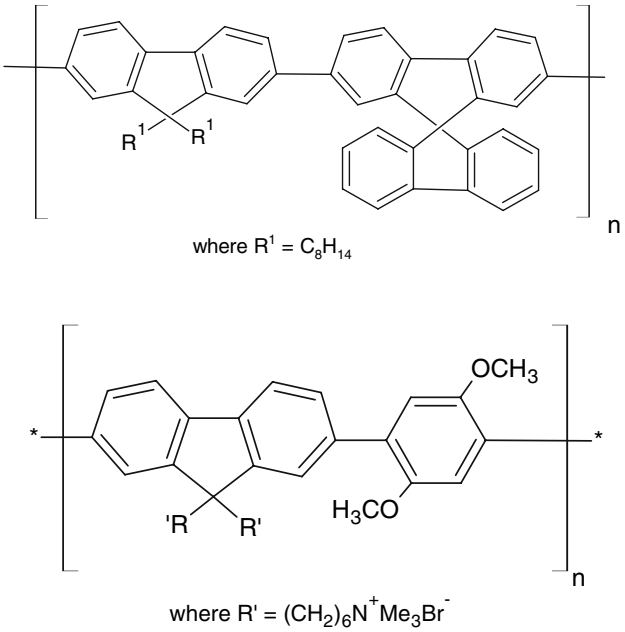

Fig. 1 The chemical structures of the polymers: poly[9,9-dioctylfluorene-*co*-*alt*-spirofluorene] (PFFS) and poly[9,9-bis(6-(*N*,*N*,*N*-trimethylammonium)-hexyl)fluorene-*co*-*alt*-2,5-dimethoxy-1,4-phenylene dibromide (PFPB)

Experiments

The active polymer used in this study is poly[9,9-dioctylfluorene-*co*-*alt*-spirofluorene] (PFSF). Both the PFSF and PFPB polymers were synthesized in the Department of Chemical and Biomolecular Engineering, National University of Singapore. In the solid state, both polymers have a flaky, pale yellow appearance. Figure 1 shows the chemical structure of the polymers. Both the PFSF and PFPB polymer solution (10 mg/mL) were prepared by dissolving every 10.0 mg of PFPB in 1.0 mL of toluene. It was stirred in an ultrasonic bath (Sonic Clean 250HT) for 30 min and then filtered using Whatman 0.1 μm filters.

The devices were fabricated with the configuration of ITO/PEDOT:PSS/PFSF/PFPB/Ca/Ag. Devices of ITO/PEDOT:PSS/PFSF/Ca/Ag without PFPB were also fabricated for comparison. Commercially available ITO-coated glass substrates were cleaned by sonicating and rinsing in acetone, methanol and deionized water, followed by oxygen plasma treatment. The hole-transporting PEDOT:PSS layer (20 nm) was spin-coated onto ITO, followed by spinning coating of the emitting polymer PFSF layer and a PFPB layer (90 nm) from a polymer solution in toluene (7.5 wt.%). Calcium (20 nm) and silver (200 nm) contacts were deposited sequentially by thermal evaporation through a shadow mask. Thermal evaporation was carried out in ULVAC system at a base pressure of 2.0×10^{-6} Torr. The fabricated devices were protected by encapsulation of a capping glass sealed with epoxy.

The current density–luminance–voltage (*J*–*L*–*V*) curves were measured using a fully computer-controlled system consisting of a dynamic multimeter (Keithley DMM 2001), a source meter (Keithley 3A 2420) and eight calibrated Si photodiodes. The software was based on LabView. Device lifetime, noise spectrum and EL spectrum were performed simultaneously by driving the devices with low noise constant current of 1 mA inside a shielded box. Noise measurements were performed using a standard DC technique. Devices were biased by a low noise DC current powered by a stack of Ni–Cd batteries. The noise signal, fluctuations of current *I*, was coupled to a wideband (0.03 Hz–100 kHz) low-noise SR570 current preamplifier. The output of the amplifier was fed to a HP35670A digital signal analyzer in which the power spectral density (PSD) *S*(*f*) of current *I* was calculated in the range of 1–800 Hz. The experiments have been repeated for 5 times in order to ensure the validation of the results.

Results and discussion

Absorption and photoluminescence spectra analysis

The absorption and photoluminescence (PL) spectra of PFPB in methanol and in film forms were studied and are shown in Fig. 2. The absorption spectrum of PFPB in

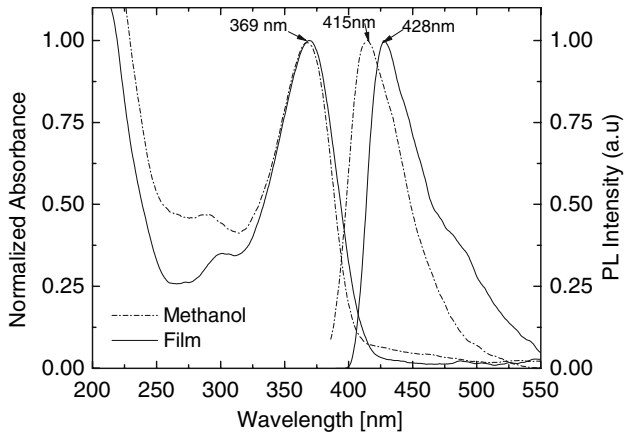

Fig. 2 Absorption and photoluminescence spectra of PFPB in methanol and in films

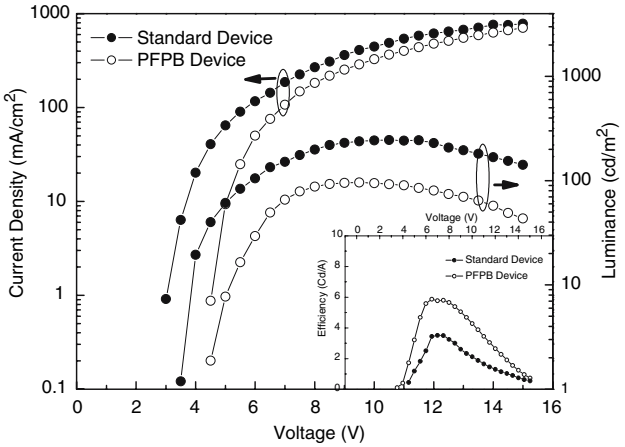

Fig. 3 Current–voltage–luminescence characteristics based on device structures: ITO/PEDOT:PSS/PFSF/PFPB/Ca/Ag and ITO/PEDOT:PSS/PFSF/Ca/Ag. The inset shows the efficiency curves for the above device structures

methanol shows a strong band peaked at 369 nm and the PL spectrum shows a peak at 415 nm without any vibronic features. There is no significant change in the absorption spectrum of PFPB in the film state as compared to the absorption spectrum in methanol. The PL spectrum of PFPB in film shows a band peaked at 428 nm with a weak vibronic shoulder at around 490 nm. This indicates that the excited state conformation of PFPB in film states is slightly different compared to the PL spectrum in solution, which could be attributed to the weak interchain interaction in the film states. The effect of thermal annealing on the film spectral properties was also studied. The spectral position did not change when the annealing temperature was increased up to 190 °C. This indicates that there is no film morphological change with the temperature changes. The band gap of the polymer was estimated from the absorption edge as 3.02 eV. The photoluminescence quantum efficiency of this polymer in methanol was estimated using quinine sulfate as a reference to be 69.6%.

Device current density–voltage–luminescence and lifetime characteristics

PLEDs were fabricated using PFPB as an electron transport layer (ETL) with the device configuration of ITO/PEDOT:PSS/PFSF/PFPB/Ca. For comparison, the PLED devices were fabricated with PFSF (chemical structure shown in Fig. 1) as an emissive layer without PFPB as an ETL layer. The devices fabricated with PFSF polymer in the absence and presence of ETL PFPB are named as **P1** and **P2** device, respectively. The luminescence–voltage (*L*–*V*) and current density–voltage (*J*–*V*) characteristics of the devices are shown in Fig. 3. Both devices showed a low turn-on voltage of around 4.0 V. The brightness of 100 and 300 Cd/cm^2 was achieved for **P1** and **P2** at 8 V, respectively. The inset of Fig. 3 shows the current efficiency with voltage (η–*V*) for the devices. It is evident that device **P2** displays higher current efficiency than **P1**. Figure 4 shows the voltage and electroluminance intensity as a function of operation time for devices when driven continuously at a constant current of 1 mA. The result shows that device **P2** has much longer lifetime as compared to that for **P1**, as indicated by 20 Cd/m^2 luminance remained after 50 h driven with a constant current.

The increase in current and luminescence efficiency with PFPB as an ETL is due to the reduction of barrier for electron injection at the cathode/polymer interface [9]. Most luminescent conjugated polymers are p-type and hole mobility is much larger than electron mobilities. The barrier for electron injection from the cathode is relatively large as compared to the barrier for hole injection from the anode, precluding balanced charge transport in the devices. This issue can be addressed by the introduction of an ETL between the luminescent polymer and the

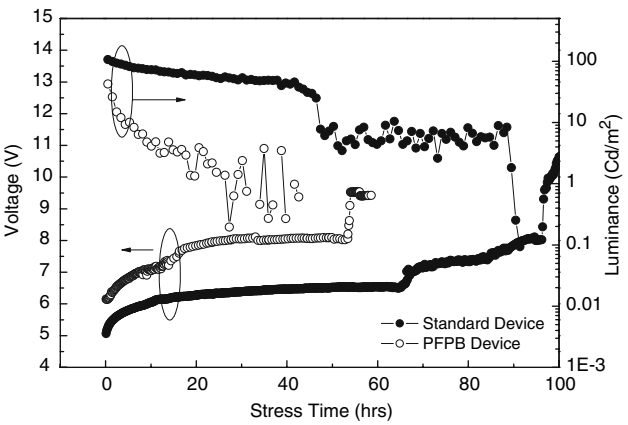

Fig. 4 The lifetime curves for the device structures: ITO/PEDOT:PSS/PFSF/PFPB/Ca/Ag and ITO/PEDOT:PSS/PFSF/Ca/Ag

cathode, which will facilitate electron injection. N-type electron-transporting polymers are commonly used as the ETL materials. They have high electron affinities which reduce the barrier for electron injection at the cathode/polymer interface. Furthermore, ETL can separate the radiative recombination zone from the cathode so that recombination at the cathode/polymer interface is avoided [10]. Both non-conjugated polymers, such as the oxadiazole-containing side-chain polymers and conjugated polymers such as poly(cyanoterephthalylidene)s, poly(phenylquinoxaline)s, polypyridines, and polyquinolines have been reported as suitable ETL materials [11]. The addition of ETL has demonstrated significant improvements in EL efficiency and brightness [12]. PLEDs with an ETL and high work function metal cathodes such as Al demonstrated similar efficiencies to those devices using low work function metals such Ca or Ba as the cathode [13]. This utilization is important as it significantly enhances electron injection in combination with the use of air stable cathode.

Device low frequency noise characteristics

The low frequency noise characteristics of the PLED devices were studied and the results are shown in Fig. 5. Figure 5a shows the variation of noise level with time at 64 Hz for both devices. For **P1** devices, after ca. 20 h, the noise level suddenly increased $\sim$4 orders of magnitude. The noise signal fluctuated dramatically. For **P2** devices, however, there is no obvious amplitude increase in the noise spectra within the first 50-h operation. Thereafter, the noise amplitude increased $\sim$3 orders, which indicates the oncoming failure for device. The inset of Fig. 5a depicts the initial 1/*f* noise of devices fabricated for **P1** devices and **P2** devices, where devices were driven at a constant current of 1 mA. From the LFN results, the slopes for **P1** devices and **P2** devices are extracted as 1.41 and 1.19, respectively. **P1** devices show a larger noise amplitude with a larger low frequency noise slope. Figure 5b shows the low frequency noise slope change versus stress time for **P1** and **P2** devices. It shows that **P1** devices have a much higher slope value, while **P2** devices show an increasing noise slope from 1.2 to 1.45. The low frequency noise spectral versus stress time is shown in the inset of Fig. 5b for reference.

Devices **P1** and **P2** with a similar current-voltage behavior exhibited different low frequency noise characteristics, which is primarily because the current–voltage behavior represents a macroscopic description of the device characteristics, while low frequency noise is a sensitive probe of defects, non-uniformities, surface velocity fluctuations, etc., due to incomplete bonding or defect sites at surfaces or interfaces. At the beginning of

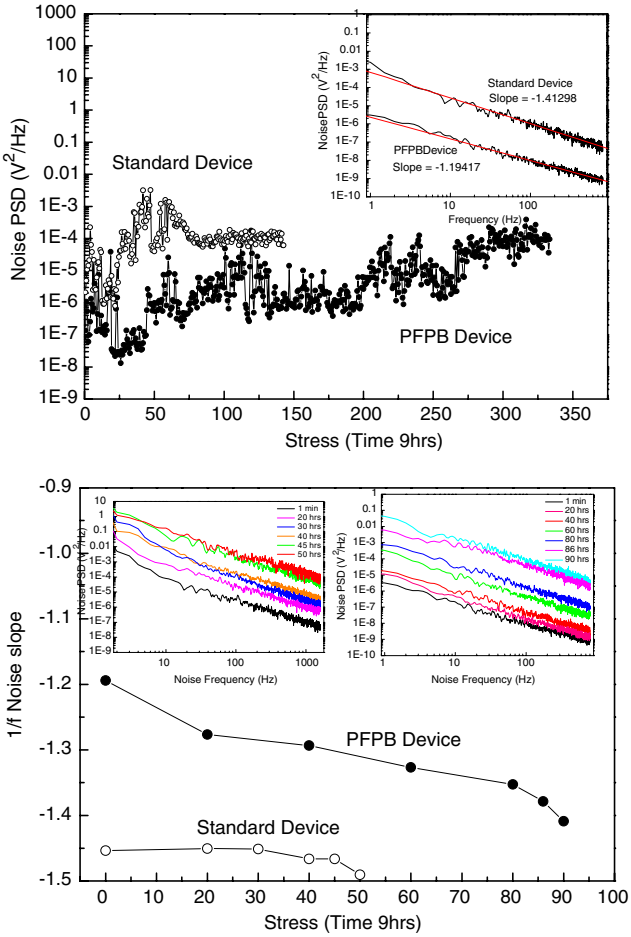

Fig. 5 (**a**) 1/*f* noise PSD level at 64 Hz vs. time for device structures: ITO/PEDOT:PSS/PFSF/PFPB/Ca/Ag and ITO/PEDOT:PSS/PFSF/Ca/Ag. The inset shows the initial 1/*f* noise of devices when driven at a constant current of 1 mA. The Hooge's coefficient α values are 1.61603 and 1.12191, respectively, for devices ITO/PEDOT:PSS/PFSF/PFPB/Ca/Ag and ITO/PEDOT:PSS/PFSF/Ca/Ag. (**b**) 1/*f* noise slope vs. time for different device structures: ITO/PEDOT:PSS/PFSF/PFPB/Ca/Ag and ITO/PEDOT:PSS/PFSF/Ca/Ag. The inset shows the 1/*f* noise spectra of the devices vs. time for devices ITO/PEDOT:PSS/PFSF/PFPB/Ca/Ag and ITO/PEDOT:PSS/PFSF/Ca/Ag

driving, by monitoring device LFN spectrum, we can predict device lifetime, interface quality, and bulk material quality.

On the basis of our previous work on LFN characteristics of OLEDs, two noise components are present in the low frequency noise spectrum [14]: 1/*f* Gaussian noise from bulk materials which has a slope of 1, and excessive frequency noise related to device interfaces or defects and traps, resulting in a slope larger than 1. The noise slope (the interface) is the primary indication of device lifetime, i.e. the quality of the interface (noise slope) primarily determines lifetime in comparison with the bulk quality (noise magnitude). Noise spectral analysis is a good way to comprehend the device interface (noise slope) and bulk

quality (noise magnitude). Larger spectral slope for device **P1** observed in the inset of Fig. 5a, indicating relatively poorer interfaces of **P1** devices than **P2** devices. Smaller spectral slope of **P2** devices predicted a longer lifetime. During the device driving, LFN technique is proved to be a good in situ monitoring tool. The sudden noise amplitude increase may predict bulk material degradation occurring inside the devices. The sudden fluctuation of the noise signal may predict the device catastrophe failure. The increase of the noise slope change may also be related to the material degradation inside the devices. Large $1/f$ noise slope can be explained by the fluctuations in the number of charge carriers. In OLEDs, interface deterioration has been ascertained to play an important role in device degradation [14]. On the other hand, interface deterioration definitely causes energy barrier to change, resulting in fluctuation of the number of charge carriers. The other possible mechanism for carrier number fluctuations is the widely existing material defects and flaws, which are primarily reflected by the magnitude of noise PSD. The defects inside electroluminescent materials could come from the synthesis and purification processes, which decrease the carrier injections and cause increased low frequency noise level. During device driving, an increase in LFN slope was observed for device **P1** after 40 h, which indicates the fluctuation of carrier number, the generation of traps and defects, and the ongoing deterioration in the interface. The acceleration in the slope change shows the relaxation of excited electron into higher vibronic energy levels of the HOMO after long-time driving (ca. 140 h), which was reflected in the slightly red-shifted (~20 nm) maximum wavelength in the emission spectra. On the basis of the above-mentioned discussion, it shows that the noise spectra are not only a good tool for device quality description ad lifetime predication but also a good in situ device characterization method.

The spectral stability of PLEDs

The spectral stability of OLEDs remains a challenge for polyfluorene-based materials. Figure 6 shows the spectral change of **P1** devices and **P2** devices with time elapse. The inset in Fig. 6 shows the peak intensity decay versus stress time and the center wavelength changes versus stress time. The **P1** devices display pure green emission with a maximum emission centered at 430 nm and a weak orange emission at 500 nm. However, the center wavelength fluctuated after stress of 10 h. By contrast, **P2** devices display a mixed yellow-orange emission with a strong yellow emission at 500 nm. The EL spectra remain relatively stable in both the maximum wavelength and shape even after ca. 60 h driving, indicating the suppression of

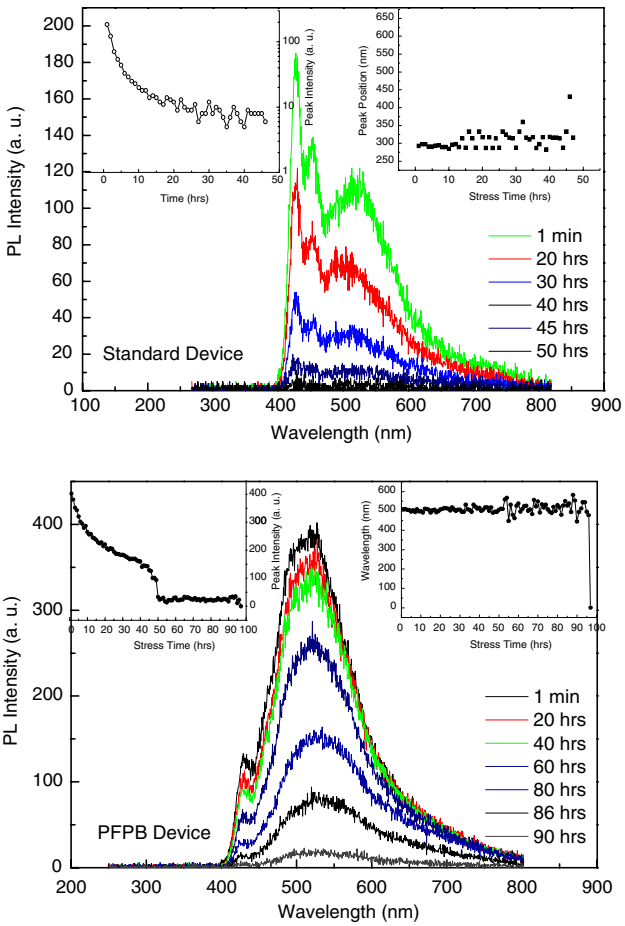

Fig. 6 (**a**) The spectral curves with time elapse for the device of ITO/PEDOT:PSS/PFSF/Ca/Ag. The left inset shows the peak intensity decreases with the time elapse and the right inset shows the peak position vs. the time elapse. (**b**) The spectral curves with time elapse for device of ITO/PEDOT:PSS/PFSF/PFPB/Ca/Ag. The left inset shows the peak intensity decreases with the time elapse, the right inset shows the peak position vs. the time elapse

troublesome excimer formation and thus resulting in a stable green emission for **P2** devices.

When we compare the EL spectra between **P1** and **P2** devices, it is found that **P1** shows a heavily structured and broad PL spectrum, which contains a shoulder at around 500 nm and a long tail beyond 600 nm. When the rigid thieno[3,2-*b*]thiophene ring (here is not right) is incorporated into the backbone of polyfluorene (**P2**), narrow and stable EL emission spectra are obtained. The EL spectra of **P2** showed stable green emission (maximum emission at 500 nm) and no measurable spectral change and/or additional emission peak observed with time or driven voltage. Furthermore, the EL emission spectra of **P2** have a FWHM (full width at half-maximum) of only ~70 nm, a good resolution for display application.

In Summary, **P2** device demonstrates better performance in terms of higher current efficiency, smaller LFN

noise slope, stable and narrower emission spectra as compared to **P1** device.

Conclusions

The electrical and optical properties of an alcohol soluble aminoalkyl-substituted cationic conjugated polymer PFPB have been investigated. PFPB is blue-emitting, with long alkyl side chains and two methoxy side chains. PLEDs were fabrication using PFPB as an electron injection layer and the device physics were studied. The improvement in the emission spectral quality of the device (narrower spectra and weaker tail extending to a longer wavelength direction) compared to that of the device without PFPB indicates that PFPB can be used as an ETL to improve the PLED performance. The interface between the cathode and the emissive layer is improved through the introduction of a PFPB layer. Results in this report indicate that the poly(fluorene-*co*-phenylene)-based water/alcohol soluble cationic conjugated polymer avoids the intermixing between the polymer and adjacent ETL layer which is a common and serious problem in fabrication of multilayer PLEDs by solution casting methods. This makes alcohol solubility materials attractive for applications in fabricating PLEDs.

Acknowledgements The authors acknowledge National University of Singapore to provide research grants associate with polymer development. Grant No.: R279-000-221-305 and R279-000-197-112/133.

Appendix: Synthesis of the polymers

Poly(9,9-bis(6′-bromohexyl)fluorene-*co-alt*-2,5-dimethoxy-1,4-phenylene)

2,7-Bis[9,9′-bis(6″-bromohexyl)-fluorenyl]-4,4,5,5-tetramethyl-[1.3.2]dioxaborolane (372 mg, 0.5 mmol), 1,4-dibromo-2,5-dimethoxybenzene (148 mg, 0.5 mmol), $Pd(PPh_3)_4$ (5 mg), and potassium carbonate (830 mg, 6 mmol) were placed in a 25 mL round bottom flask. A mixture of water (3 mL) and toluene (5 mL) was added to the flask and the reaction vessel was degassed. The mixture was vigorously stirred at 85 °C for 24 h and then precipitated into methanol. The polymer was filtered and washed with methanol and acetone, and then dried under vacuum for 24 h to afford the polymer (240 mg, 76%) as white fibers. ^{1}H NMR (200 MHz, $CDCl_3$): δ 7.8–7.1 (m, 8H), 3.8 (s, 6H), 3.3–3.2 (t, 4H), 2.1 (m, 4H), 1.7 (m, 4H), 1.3–1.2 (m, 8H), 0.9 (m, 4H). ^{13}C NMR (50 MHz, $CDCl_3$): δ 151.3, 150.7, 140.2, 137.2, 132.4, 128.3, 124.7, 119.7, 115.7, 57.2, 55.2, 40.4, 34.2, 33.0, 29.5, 28.1, 24.2.

Poly[9,9-bis(6′-*N*,*N*,*N*,-trimethylammonium)hexyl) fluorene-*co-alt*-2,5-dimethoxy-1,4-phenylene) dibromide]

Condensed trimethylamine (2 mL) was added dropwise to a solution of the neutral polymer 2a (70 mg) in THF (10 mL) at −78 °C. The mixture was allowed to warm up to room temperature. The precipitate was redissolved by the addition of water (10 mL). After the mixture was cooled down to −78 °C, extra trimethylamine (2 mL) was added and the mixture was stirred for 24 h at room temperature. After removing most of the solvent, acetone was added to precipitate the polymer (80 mg, 83%) as an off-white powder. ^{1}H NMR (50 MHz, CD_3OD): δ 7.8–7.6 (m, 8H), 3.9 (s, 2H), 3.3–3.2 (m, 4H), 3.1 (s, 18H), 2.2 (br, 4H), 1.6 (br, 4H), 1.3 (br, 8H), 0.8 (br, 4H). ^{13}C NMR (50 MHz, CD_3OD): δ 152.5, 151.7, 141.6, 138.7, 132.3, 129.6, 126.3, 120.8, 116.5, 67.8, 57.6, 56.4, 53.6, 31.0, 30.5, 27.0, 25.0, 23.7.

Poly[(9,9-dioctylfluorene-2,7-diyl)-*alt-co*-(9,9′-spirofluorene-2,7-diyl)]

A mixture of 2,7-dibromofluorene-9,9′-spirobifluorene (234 mg, 0.5 mmol) and 2,7-bis[9,9′-dioctylfluorenyl]-4,4,5,5-tetramethyl-[1.3.2]dioxaborolane (381 mg, 0.5 mmol), $Pd(PPh_3)_4$ (5 mg) and potassium carbonate (830 mg, 6 mmol) were placed in a 25 mL round bottom flask. A mixture of water (3 mL) and toluene (5 mL) was added to the flask and the reaction vessel was degassed. The mixture was vigorously stirred at 85 °C for 24 h and then precipitated into methanol. The polymer was filtered and washed with methanol and acetone, and then dried under vacuum for 48 h to afford the product (288 mg, 80%) as white fibers. ^{1}H NMR (300 MHz, $CDCl_3$, ppm): δ: 7.93–7.53 (m, 8H), 7.42–6.87 (m, 12H), 1.90 (br, 4H), 1.20–0.90 (m, 20H), 0.75 (t, 6H), 0.60 (br, 4H). ^{13}C NMR (75 MHz, $CDCl_3$, ppm): δ 151.5, 149.8, 148.8, 141.9, 141.4, 140.5, 139.9, 139.7, 127.9, 127.8, 127.1, 126, 124.3, 122.4, 121.2, 120.2, 120.1, 119.7, 55.2, 40.2, 31.7, 29.9, 29.2, 29.1, 23.7, 22.6, 14.0.

References

1. Kiess H (1992) Conjugated conducting polymer. Springer-Verlag, New York
2. Burroughes JH, Bradley DDC, Brown AR, Marks RN, Mackay K, Friend RH, Burns PL, Holmes AB (1990) Nature 347:539
3. Huang F, Wu H, Wang D, Yang W, Cao Y (2004) Chem Mater 16:708
4. Elsenbaumer RL, Jen KY, Oboodi R (1986) Synth Metals 15:169
5. Ramey MB, Hiller J, Rubner MF, Tan C, Schanze KS, Reynolds JR (2005) Macromolecules 38:234

6. Balanda PB, Ramey MB, Reynols JR (1999) Macromolecules 32:3970
7. Ma W, Iyer PK, Gong X, Liu B, Moses D, Bazan GC, Heeger AJ (2005) Adv Mater 17:274
8. Liu B, Yu W, Lai Y, Huang W (2000) Chem Commun 551
9. Wu H, Huang F, Mo Y, Yang W, Wang D, Peng J, Cao Y (2004) Adv Mater 16(20):1826
10. Yang Y, Pei Q (1995) J Appl Phys 77(9):4807
11. Groenendaal LB, Jonas F, Dieter F, Pielartzik H, Reynolds RR (2000) Adv Mater 12(7):481
12. Hwang MY, Hua MY, Chen SA (1999) Polymer 40:3233
13. Huang F, Hou L, Wu H, Wang X, Shen H, Cao W, Yang W, Cao Y (2004) J Am Chem Soc 126:9845
14. Ke L, Zhao XY, Kumar RS, Chua SJ (2006) IEEE Electron Device Lett 27(7):555